

Bootstrapping traceless symmetric $O(N)$ scalars

Marten Reehorst^{a,b}, Maria Refinetti^{a,c}, Alessandro Vichi^{a,d}

^a *Institute of Physics, École Polytechnique Fédérale de Lausanne (EPFL),
Rte de la Sorge, BSP 728, CH-1015 Lausanne, Switzerland*

^b *Institut des Hautes Études Scientifiques, Bures-sur-Yvette, France*

^c *Laboratoire de Physique de l'École Normale Supérieure, Université PSL, CNRS,
Sorbonne Université, F-75005 Paris, France*

^d *Dipartimento di Fisica dell'Università di Pisa and INFN,
Largo Pontecorvo 3, I-56127 Pisa, Italy*

Abstract

We use numerical bootstrap techniques to study correlation functions of traceless symmetric tensors of $O(N)$ with two indices t_{ij} . We obtain upper bounds on operator dimensions for all the relevant representations and several values of N . We discover several families of kinks, which do not correspond to any known model and we discuss possible candidates. We then specialize to the case $N = 4$, which has been conjectured to describe a phase transition in the antiferromagnetic real projective model ARP^3 . Lattice simulations provide strong evidence for the existence of a second order phase transition, while an effective field theory approach does not predict any fixed point. We identify a set of assumptions that constrain operator dimensions to a closed region overlapping with the lattice prediction. The region is still present after pushing the numerics in the single correlator case or when considering a mixed system involving t and the lowest dimension scalar singlet.

Contents

1	Introduction	3
1.1	RP^{N-1} and ARP^{N-1} models	3
1.2	The Landau-Ginzburg-Wilson effective action	5
1.3	Scalar gauge theories	6
2	Setup	7
2.1	The $t \times t$ OPE	8
2.2	4pt functions and the crossing equations	9
2.3	Setup of mixed $t - s$ bootstrap	10
3	A systematic study of general N	12
3.1	Bounds on operator dimensions	12
4	Focusing on $O(4)$	19
4.1	Bounds on operator dimensions and OPE coefficients	21
4.2	Isolating the ARP^3 model	25
4.3	Results mixed t-s bootstrap	27
5	Conclusions	29
A	2pt and 3pt functions	30
B	Four point tensor structures	32
C	$O(N)$ vs $O(N(N + 1)/2 - 1)$ vector bootstrap.	34
D	Additional Plots	38
E	Parameters of the numerical implementation	43

1 Introduction

The conformal bootstrap [1, 2] (see [3, 4] for a review) has successfully classified many 3D CFTs, providing stringent predictions of operator dimensions, which translate in precise determinations of the corresponding critical exponents [5–11]. These techniques have been used to study many problems including multiple scalars [12–17], fermions [18–20], currents [21, 22], stress tensors [23] and various global symmetry representations [24–44].

In this work we push this program further and explore the space of three dimensional conformal field theories (CFTs) containing a scalar operator t_{ij} , which is a traceless symmetry tensor of $O(N)$ with rank-2. While such operators are also present in the well studied $O(N)$ -vector models, here we want to target fixed points of gauge theories, where the operator t_{ij} can arise as the simplest gauge invariant scalar made from more elementary fields, charged under the gauge symmetry.

Similar studies have been done for adjoint representations of $SU(N_f)$ in four dimensions, with application to the conformal window of QCD-like theories. In that case, however, bootstrap bounds have not revealed any surprise [37, 38]. On the contrary, the present setup will show many interesting features.

In addition to the general exploration of CFTs, in the present work we also address the existence of a fixed point observed in the antiferromagnetic real projective model with N components ARP^{N-1} , in the specific case $N = 4$. Lattice simulations present strong evidences of a second order phase transition, driven by an order parameter transforming in the rank-2 representation of $O(4)$; on the contrary, an effective approach based only on the Landau-Ginzburg-Wilson paradigm seems to disagree [45]. We will present bootstrap evidences confirming the existence of a fixed point. We will also discuss new prediction for certain operator dimensions and OPE coefficients that could be tested by future lattice studies.

Before entering in the bootstrap setup and present our results, let us broadly discuss what theories must be consistent with our bootstrap bounds. The following analysis will also guide us through the choice of reasonable assumptions to isolate theories of interest.

1.1 RP^{N-1} and ARP^{N-1} models

We begin with a simple lattice model, the $(A)RP^{N-1}$, which is defined as a system of spins \mathbf{s}_x taking values in the real projective space RP^{N-1} , with the index x labelling the lattice site.

Equivalently, we can describe the system by considering \mathbf{s}_x to take values in \mathbb{R}^N , with the restriction $\mathbf{s}_x \cdot \mathbf{s}_x = 1$ and the identification $\mathbf{s}_x \sim -\mathbf{s}_x$; the latter condition can be viewed as a \mathbb{Z}_2 gauge symmetry, since one can change sign to each spin independently, i.e. locally. The hamiltonian can be written as

$$H_{RP^{N-1}} = J \sum_{\langle x,y \rangle} |\mathbf{s}_x \cdot \mathbf{s}_y|^2 \quad (1)$$

where $\langle \mathbf{x}, \mathbf{y} \rangle$ indicates that the sum runs over pairs of nearest neighbors. For negative J the system is ferromagnetic while for positive J it is antiferromagnetic. This model has been studied in the antiferromagnetic regime and for $N \leq 4$ using lattice simulations [45]. It was found that for $N = 2, 3$ the IR admits a second order phase transition, and the IR fixed point seems to be in the same universality class of the $O(2)$ and $O(5)$ model respectively. The case $N = 4$ is particularly interesting, since it still presents evidences of a second order phase transition but this time the critical exponents do not correspond to those of the $O(m)$ -model, for any m . Moreover the transition appears to be driven by an order parameter transforming in the traceless symmetric representation of $O(4)$.

Let us briefly discuss the structure of the order parameter, as it will be useful also for the discussion in the next sections. In the *ferromagnetic* case, the energy is minimized by aligning the directions of the spins. Thus, at low energy the system breaks $O(N)$ symmetry by aligning in a preferred direction. This configuration preserves translational invariance. In the standard LGW approach one looks for a gauge invariant order parameter that is non-zero in the ordered phase and vanishes in the disordered phase. This order variable is built from the *site variable*, $P_x^{ab} = s_x^a s_x^b - \delta^{ab}/N$. We then define the order parameter as its sum over lattice sites $M^{ab} = \sum_x P_x^{ab}$. We see that in the ordered phase the contributions to M^{ab} are cumulative, due to the preferred direction, resulting in a non-zero matrix. At high temperature, in the isotropic phase, contributions will cancel so that $M^{ab} \rightarrow 0$ in the infinite temperature limit. This order parameter transforms as a traceless symmetric representation of $O(N)$ and is invariant under a lattice symmetry that interchanges two sublattices.¹

In the *antiferromagnetic* case the energy is instead minimized by taking $\mathbf{s}_x \cdot \mathbf{s}_y = 0$ for neighboring sites. Thus, in the ordered phase every spin is orthogonal to its nearest neighbor. Unlike anti-correlation in the usual ferromagnetic case, here one can divide the lattice in two sublattices, and the spins are orthogonal among the two. Orthogonality does not fix the configuration uniquely unlike correlation or anti-correlation. Thus, it is not immediately clear what the symmetries of the ordered state are and what order parameter has a non-zero expectation value in the ordered phase. In [46], for the similar case of CP^2 , it was shown that the order parameter must also break the symmetry that interchanges the sublattices. This proof can easily be extended to the case of ARP^2 . Unfortunately we don't know of any proof for $N > 2$. If we assume the same holds for general N the correct order parameter is built from a staggered site variable $A_x^{ab} = p_x P_x^{ab}$, where $p_x = \exp[i\pi \sum_{k=1}^3 x_k]$, i.e. the parity of the lattice site. Summing over the staggered site variable the order parameter is given by $M^{ab} = \sum_{\mathbf{x}} A_{\mathbf{x}}^{ab}$. This order parameter also transforms as a traceless symmetric representation of $O(N)$ but this time is odd under the \mathbb{Z}_2 symmetry.

¹Gauge invariance forbids a linear order parameter s_x^a so the next simplest order parameter is quadratic. The vanishing of the order parameter in the disordered phase forces the subtraction of the trace resulting in the traceless symmetric representation.

The lattice analysis² for ARP^3 led to the following estimates of the critical exponents:

$$\Delta_s = 3 - \frac{1}{\nu} = 1.28 \pm 0.13, \quad \Delta_t = \frac{1 + \eta}{2} = 0.54 \pm 2, \quad \Delta_{s'} > 3 \quad (\text{lattice results [45]}) \quad (2)$$

1.2 The Landau-Ginzburg-Wilson effective action

In many cases of physical interest one can understand the critical behavior of a lattice system also starting from a UV description in terms of a field theory of a scalar field with only a few renormalizable interactions. Thanks to the properties of the RG flow, if the two UV theories belong to the same universality class, they will flow to the same fixed point in the IR.

Physically this is equivalent to identifying the order parameter that describes the fluctuations near criticality and writing an effective Hamiltonian. The order parameter is chosen such that it vanishes in the disordered phase and is non-zero in the ordered phase. Thus, it is expected to be small near criticality and it make sense to consider only the leading terms.

If one is interested in describing the phase transition observed for ARP^{N-1} , the order parameter Φ_{ij} is a traceless symmetric rank-2 tensor of $O(N)$, odd under an additional \mathbb{Z}_2 symmetry. The LGW Hamiltonian reads:

$$\mathcal{H} = \text{Tr}(\partial_\mu \Phi)^2 + r \text{Tr} \Phi^2 + u_0 (\text{Tr}(\Phi^2))^2 + \frac{v_0}{4} \text{Tr} \Phi^4 \quad (3)$$

The analysis of the β -functions for the couplings u_0 and v_0 in ε -expansion at one loop reveals the existence of four fixed points. Two of them are well known: the free Gaussian theory ($u_0^* = v_0^* = 0$) and the $O(N')$ Wilson-Fisher fixed point ($v_0^* = 0$), with $N' = N(N + 1)/2 - 1$ the total number of scalars encoded in the tensor Φ . In addition there are two fixed points, with both coupling non-zero, that merge at $N = N_c$ and turn complex for $N > N_c$. A Borel resummation of the five-loop ε -expansion predicts $N_c \approx 3.6$ [45]. For $N = 2, 3$ the additional relation $\text{Tr} \Phi^4 = (\text{Tr} \Phi^2)^2/2$ holds. So even for $N < N_c$ the new fixed points can be mapped respectively to the $O(2)$ and $O(5)$ model. In conclusion, the LGW analysis predicts that no fixed point exist for this model besides the WF ones. This is in tension with the lattice results discussed in the previous section.

²The analysis of [45] used finite-size-rescaling to study the RG invariant $R_\xi = \frac{\xi}{L}$, where ξ is the correlation length and L the lattice's size. It is observed that lines of different L 's meet at a critical temperature $\beta_c = 6.779(2)$ and the critical exponent $\nu = 0.59(5)$ was estimated. The error is due to different methods of fitting the data, while the statistical error is much smaller. Moreover, they were able to extract the critical exponent $\eta = 0.08(4)$ by analyzing the behavior of the susceptibility around the fixed point. Finally, a study of the Binder parameter shows sizeable corrections due to scaling possibly indicating an un-tuned singlet with a dimension that is close to relevant. However, the data was insufficient to give a reliable estimate on the corresponding critical exponent.

1.3 Scalar gauge theories

Traceless symmetric tensor of $O(N)$ can arise in a many different theories. Hence, a general bootstrap analysis will be sensitive to all of them. As an example, in this section we review the known results for a model based on a theory with local $O(M)$ gauge invariance and global $O(N)$ (see for instance [47, 48] and reference therein).

$$\begin{aligned} \mathcal{L} &= -\frac{1}{4}F_{\mu\nu}^a F^{a\mu\nu} + \frac{1}{2} \sum_{i=1} (D_\mu \phi_i)^\alpha (D^\mu \phi_i)^\alpha + V(\phi_i^a), \\ (D_\mu \phi_i)^\alpha &= \partial_\mu \phi_i^\alpha - (T^b)^\alpha_\beta \phi_i^\beta A_\mu^b, \quad V(\phi_i^a) = u_0 S^2 + v_0 \sum_{i,j} Q_{ij} Q_{ij}, \\ S &= \sum_{a,k} (\phi_k^\alpha \phi_k^\alpha), \quad Q_{ij} = \sum_a \phi_i^\alpha \phi_j^\alpha - \frac{1}{N} \delta_{ij} S \end{aligned} \quad (4)$$

where μ and ν are spacetime indices, $\alpha, \beta, \gamma = 1, \dots, M$ are fundamental indices of the gauge group $O(M)$, $a, b, c = 1, \dots, M(M-1)/2$ are adjoint indices and $i, j, k = 1, \dots, N$ are indices of the global flavor group. The presence of a gauge symmetry imposes that, at the fixed points, local operators must be made from gauge invariant combinations of the fields ϕ_i^α and the field strength $F_{\mu\nu}^a$. In particular the smallest dimensions scalars are the singlet S and the traceless symmetric $O(N)$ tensor Q_{ij} defined in (4).

The above models have been extensively studied: the ε -expansion [48] predicts the existence of a fixed point only for

$$N > 44(M-2). \quad (5)$$

Moreover, the ε -expansion shows that the gauge invariant model is always stable compared to the enhanced $O(NM)$ model. Alternatively, one can study the model in 3d, in the large- N limit at fixed M . For instance one obtains [47]:

$$\begin{aligned} \Delta_S &= 1 + \frac{16}{3\pi^2 N} (9M-7) + O\left(\frac{1}{N^2}\right), \\ \Delta_Q &= 1 - \frac{16}{3\pi^2 N} (3M-5) + O\left(\frac{1}{N^2}\right), \end{aligned} \quad (6)$$

Clearly the above expressions cannot be trusted at small values of N . Nevertheless one could compare these expressions with the bootstrap bounds. The main issue is that, given N , there are in principle infinitely many underlining gauge theories with the same global symmetry but different CFT-data, as shown already by the leading corrections in Eq. (6).³

Let us conclude this overview by discussing a few basic differences among the theories discussed so far. First of all, in presence of a continuous gauge symmetry, the spectrum of the CFT will be richer, given the presence of extra states such as glue-balls $(F_{\mu\nu}^a)^2$

³Note that (6) has been obtained in the limit of large N , while keeping M fixed. If instead one consider $M \sim N$ then the expansion would change.

or combination of the two fundamental fields.⁴

On the contrary, if the gauge symmetry is discrete, as for instance the discrete \mathbb{Z}_2 gauge symmetry of RP^N models, we do not expect these extra states.

Interestingly, this is not the only difference. Consider for instance the smallest operator transforming in the representation described by a squared Yang-tableau with four boxes, $\begin{array}{|c|c|} \hline \square & \square \\ \hline \square & \square \\ \hline \end{array}$. We call it the *Box* representation. We will see in the next section that such representation appears in the OPE of two rank-2 tensors. In a gauge theory like in (4), the smallest scalar in the Box representation is given by

$$\mathcal{O}_{ij,kl} \sim Q_{ik}Q_{jl} - Q_{il}Q_{jk} - \text{traces}, \quad (7)$$

The non-triviality of this operator is guaranteed by the internal gauge indices. However, if these were absent, one could not construct it: given a real scalar operator s_i the smallest non trivial operator in the Box representation that one can construct requires two derivatives

$$\mathcal{O}'_{ij,kl} \sim J_{ik}^\mu J_{\mu jl}, \quad J_{ij}^\mu = s_i \partial^\mu s_j - s_j \partial^\mu s_i, \quad (8)$$

or more fields. This reasoning is valid only in a neighborhood of the UV description, however it gives us an intuition about which operators we should expect in the CFT. Hence, we do not expect the IR fixed point of $(A)RP^N$ models to have light scalars in the Box representation.

More in general, the impossibility to construct light operators in a given representation can be a guiding principle to distinguish different theories, especially when gauge symmetry are involved. Let us view another example: in the LGW model the fundamental field is a traceless symmetric tensor, while in a gauge theory the fundamental field is a vector of $O(N)$, with an addition gauge index. Although ϕ_i^α is not gauge invariant, the existence of a more fundamental building block has important consequences and does have an impact on the spectrum of the CFT. For instance, for $SO(M=3)$ it is possible to construct barion-like state of the form $B_{ijk} \sim \epsilon_{\alpha\beta\gamma} \phi_{[i}^\alpha \phi_j^\beta \phi_{k]}^\gamma$, transforming in the antisymmetric representation with three indices of $O(N)$ and having a small dimension.⁵ In the LGW theory, the lightest state in same representation would be much heavier.

Finally, a major difference between the gauge model (4) and the LGW description is that the latter displays a \mathbb{Z}_2 symmetry in the UV, while the former doesn't. From the CFT point of view, this symmetry imposes the vanishing of three point functions $\langle \Phi_{ij} \Phi_{kl} \Phi_{rs} \rangle$ in a putative fixed point of the LGW model, while the correlator $\langle Q_{ij} Q_{kl} Q_{rs} \rangle$ is allowed to be non-zero in the model based on a gauge theory.

2 Setup

In this section we explain the bootstrap setup of the $\langle tttt \rangle$ correlator and its extension to the mixed $t - s$ bootstrap. We first discuss the operators that can be exchanged in

⁴Only a subset of those operators, such as glueballs, are accessible with the bootstrap setup considered in this paper.

⁵This operator is invariant under $SO(3)$ and not the full $O(3)$, however our bootstrap setup does not distinguish between $SO(M)$ and $O(M)$ symmetries and this is an equally valid theory to consider.

the $t \times t$ OPE. We then explain how to write the crossing equations and the resulting sum rules for the single $\langle tttt \rangle$ correlator. Next we present the extension to the mixed $t - s$ bootstrap. In appendix C we also show how this bootstrap setup for the traceless symmetric bootstrap of $O(N)$ is related to the vector bootstrap of $O(N')$ with $N' = N(N + 1)/2 - 1$.

2.1 The $t \times t$ OPE

We can write the $t \times t$ OPE as

$$t_{\square} \times t_{\square} = \sum_{\Delta, l} \lambda_{\Delta, l}^S S + \lambda_{\Delta, l}^{T^2} T_{\square}^2 + \lambda_{\Delta, l}^{T^4} T_{\square\square\square\square}^4 + \lambda_{\Delta, l}^{A^2} A_{\square}^2 \tag{9}$$

$$+ \lambda_{\Delta, l}^H H_{\square\square} + \lambda_{\Delta, l}^B B_{\square\square}$$

Here S , T^2 , T^4 , A^2 refer respectively to the singlet, traceless symmetric, four-index symmetric and the antisymmetric representations. H refers to the mixed symmetry $\{3, 1\}$ representation which we will call Hook representation, while B refers to the $\{2, 2\}$ representation or Box representation. In the rest of the paper we will leave out the young tableau notation and refer to a dimension Δ and spin l operator as $R_{\Delta, l}$, where $R \in \{S, T^2, T^4, A^2, H, B\}$.

Important special cases of operators are the first antisymmetric vector, i.e. the conserved current $J = A_{2,1}^2$, the first spin-two singlet, i.e. the stress tensor $T = S_{3,2}$. The first antisymmetric vector after the current will be denoted J' and the first spin-2 singlet after the stress tensor T' . Furthermore, we will refer to the first singlet scalar as s and the external traceless symmetric scalar as t . Again higher dimensional operators will be referred to by adding primes. For example s' refers to the second lowest dimensional singlet operator. t' will denote the first traceless symmetric operator other than t -itself. Similarly, the first scalar in the Box representation and the first vector in the Hook representation will be denoted by b and h respectively.

Under exchange of x_1 and x_2 the spatial part of the three point function $\langle t(x_1)t(x_2)O_{\Delta, l}(x_3) \rangle$ goes to $(-1)^l$ times itself. Thus, for even spins the global tensor structure must be symmetric under the exchange of the indices of the first and second operator, and antisymmetric for odd spins. The $\{S, T^2, T^4, B\}$ representations only allow a symmetric structure while the A and H representations only allow an antisymmetric tensor structure. Thus, the former set of representations will be exchanged for even spin and the latter set for odd spin.

Two OPE coefficients are of special interest. Ward identities relate the OPE coefficients of stress tensor T and the conserved current J respectively to the central charges C_J and C_T :

$$\frac{C_{J_{\text{free}}}}{C_J} = \lambda_{ttJ}^2 \tag{10}$$

$$\frac{C_{T_{\text{free}}}}{C_T} = \frac{\lambda_{ttT}^2}{\Delta_t^2} = \frac{\lambda_{ssT}^2}{\Delta_s^2} \tag{11}$$

In order to construct the correct $O(N)$ tensor structures for 3 and 4pt functions we used an index free notation similar to the one introduced for spacetime indices in [49].

The young tableaux describing the $O(N)$ irreps illustrate how indices corresponding to blocks appearing in the same row are symmetrized while blocks appearing in the same column are anti-symmetrized. The symmetrization of any row can automatically be enforced by contracting all indices corresponding to the same row with the same polarization vector S . Similarly, indices corresponding to the next row are contracted with U and so on (in this paper no irreps with more than two rows appear). One then only needs to enforce the anti-symmetry and tracelessness by hand. We review in details our method in appendixes A and B.

2.2 4pt functions and the crossing equations

The crossing equations are obtained in the standard way by equating the s-channel and t-channel decompositions of the 4pt-function. The 4pt-function $\langle tttt \rangle$ has six independent tensor structures, each providing a crossing equation of the form

$$\sum_{R, \mathcal{O}_R} \lambda_{12\mathcal{O}_R} \lambda_{34\mathcal{O}_R} \frac{g_{\Delta_{\mathcal{O}_R}, \ell_{\mathcal{O}_R}}^{\Delta_{12}, \Delta_{34}}(z, \bar{z})}{(z\bar{z})^{\frac{\Delta_1 + \Delta_2}{2}}} = \sum_{R', \mathcal{O}'_{R'}} \lambda_{32\mathcal{O}'_{R'}} \lambda_{14\mathcal{O}'_{R'}} \frac{g_{\Delta_{\mathcal{O}'_{R'}}, \ell_{\mathcal{O}'_{R'}}}^{\Delta_{32}, \Delta_{14}}(1-z, 1-\bar{z})}{((1-z)(1-\bar{z}))^{\frac{\Delta_3 + \Delta_2}{2}}}. \quad (12)$$

Here z and \bar{z} are the standard crossing ratios and g is the scalar conformal block. For the single correlator (of identical operators) both R and R' run over $\{S, T^2, T^4, A^2, H, B\}$ and $\Delta_{ij} = 0 \forall i, j$.

The final crossing equations for $\langle tttt \rangle$ can be written as

$$\begin{aligned} & \sum_{\mathcal{O}} \lambda_{\mathcal{O}}^2 V_{S, \Delta, \ell} + \sum_{\mathcal{O}} \lambda_{\mathcal{O}}^2 V_{T^2, \Delta, \ell} + \sum_{\mathcal{O}} \lambda_{\mathcal{O}}^2 V_{T^4, \Delta, \ell} + \\ & \sum_{\mathcal{O}} \lambda_{\mathcal{O}}^2 V_{B, \Delta, \ell} + \sum_{\mathcal{O}} \lambda_{\mathcal{O}}^2 V_{A, \Delta, \ell} + \sum_{\mathcal{O}} \lambda_{\mathcal{O}}^2 V_{H, \Delta, \ell} = 0_{1 \times 6}, \end{aligned}$$

where $V_{R, \Delta, \ell}$ is a 6 dimensional vector describing the contribution of a primary operator \mathcal{O} of dimension Δ , spin ℓ , and representation R . The vector $V_{R, \Delta, \ell}$ is expressed in terms of the usual F 's and H 's

$$\begin{aligned} H &= u^{\frac{1}{2}(\Delta_2 + \Delta_3)} g_{\Delta, \ell}^{\Delta_{12}, \Delta_{34}}(v, u) + v^{\frac{1}{2}(\Delta_2 + \Delta_3)} g_{\Delta, \ell}^{\Delta_{12}, \Delta_{34}}(u, v), \\ F &= v^{\frac{1}{2}(\Delta_2 + \Delta_3)} g_{\Delta, \ell}^{\Delta_{12}, \Delta_{34}}(u, v) - u^{\frac{1}{2}(\Delta_2 + \Delta_3)} g_{\Delta, \ell}^{\Delta_{12}, \Delta_{34}}(v, u) \end{aligned} \quad (13)$$

Here $g^{\Delta_{12}, \Delta_{34}}$ is the scalar conformal block normalized as entry 1 of Table I in [3]. In this section the only correlation under consideration is $\langle tttt \rangle$ and this simplifies to

$$\begin{aligned} H &= u^{\Delta_t} g_{\Delta, \ell}(v, u) + v^{\Delta_t} g_{\Delta, \ell}(u, v), \\ F &= v^{\Delta_t} g_{\Delta, \ell}(u, v) - u^{\Delta_t} g_{\Delta, \ell}(v, u) \end{aligned} \quad (14)$$

The crossing equations can also be represented by a 6 by 6 matrix. Its explicit form is⁶

$$M_{(tttt),O(N)} = \begin{pmatrix} F & 0 & 0 & 0 & \frac{1}{2}F(N+4)(N-1) & -FN \\ 0 & F & 0 & 0 & \frac{1}{2}F(N-2) & -\frac{FN}{2} \\ 0 & 0 & -F & 0 & \frac{1}{2}F(N+4) & -\frac{1}{2}F(N+2) \\ 0 & 0 & 0 & F & -3F & 2F \\ H & 0 & -\frac{2H(N-1)}{N} & -\frac{H(N+4)(N+6)(N-1)}{12N} & -\frac{H(N+4)(N-2)(N-1)}{4N} & -\frac{H(N+2)(N-3)(N-2)}{6N} \\ 0 & H & -\frac{H(N+4)(N-2)}{N(N+2)} & -\frac{H(N+6)(N-2)}{3N} & \frac{H(N+4)(N-2)}{N(N+2)} & \frac{H(N+4)(N-3)}{3N} \end{pmatrix} \quad (15)$$

Here rows correspond to the six different equations and columns correspond to the vectors $\{V_S, V_{T^2}, V_A, V_{T^4}, V_H, V_B\}$ in equation 13. The bootstrap problem consists of finding a positive linear functional α such that

$$\begin{cases} \alpha(V_{\mathbb{I}}) = 1 \\ \alpha(V_R) \geq 0 \quad \forall R \in \{S, T^2, T^4, A^2, H, B\}, \quad \forall \Delta_{R,\Delta,\ell} > \Delta_{R,\Delta,\ell}^* \end{cases} \quad (16)$$

If such a functional exists it excludes a spectrum with $\Delta_{R,\Delta,\ell} > \Delta_{R,\Delta,\ell}^*$. $\Delta_{R,\Delta,\ell}^*$ is usually taken to be the unitarity bound except when we try to find the maximal allowed gap for a certain operator or when we have reason to assume a gap above the unitarity bound for a theory that we are trying to isolate.

In practice the crossing equations are truncated by taking derivatives around the crossing symmetric point $z = \bar{z} = 1/2$ and the maximal number of derivatives is denoted by Λ . These truncated crossing equations are used as input in the arbitrary precision semi-definite programming solver SDPB (version 2) [50, 51]. The truncations and parameters used in the numerical implementation can be found in tables 2 and 1. The computations were managed using Simpleboot [52].

In addition to finding the feasible set of $\Delta_{R,\Delta,\ell}$ we can also find lower and upper bounds on squared OPE coefficients λ_{ttO}^2 by picking the corresponding vector V_λ to define the normalization of α , i.e. $\alpha(V_\lambda) = \pm 1$ and maximizing the objective $\alpha(V_{\mathbb{I}})$.⁷

2.3 Setup of mixed $t - s$ bootstrap

In this section we write the bootstrap equations for the system of correlators involving the traceless symmetric operator t and the leading singlet s . We will restrict ourselves to the case in which t is odd under a \mathbb{Z}_2 symmetry, since our goal is to study the ARP^3 model discussed in section 1.1. In that case the full system of crossing equations is given by the crossing equations of the correlators $\langle ttss \rangle$ and $\langle stts \rangle$, $\langle tsts \rangle$, and $\langle ssss \rangle$. Crossing equations involving three t -operators vanish because $t \times s$ can only exchange \mathbb{Z}_2 odd operators while $t \times t$ can only exchange \mathbb{Z}_2 even operators. All new correlators are constrained to exchange only a single irrep: $s \times s$ can only exchange neutral operators while $t \times s$ can only exchange operators in the T^2 irrep. The $t \times s$ OPE does not have

⁶The exact form depends on the normalization of the OPE coefficients. We are free to rescale columns by any positive factor and absorb this into the OPE coefficients. We are of course also free to rescale rows, i.e. equations, by any factor.

⁷Normalizing $\alpha(V_\lambda) = 1$ will give us an upper bound on the OPE coefficient, while $\alpha(V_\lambda) = -1$ will give a lower bound.

the permutation symmetry that the $t \times t$ OPE had and thus allows the exchange of both odd and even spin traceless symmetric operators.

Note that when we do not impose a gap forbidding the exchange of the external operator t in $t \times t$ results using this setup also hold for \mathbb{Z}_2 -even t .⁸

Restricting to the crossing equations for \mathbb{Z}_2 -odd t there are four additional crossing equations, two between $\langle sstt \rangle$ and $\langle tsst \rangle$, one from $\langle tsts \rangle$ and one from $\langle ssss \rangle$. The crossing equations can now be written as

$$\sum_{\mathcal{O}} (\lambda_{tt\mathcal{O}} \ \lambda_{ss\mathcal{O}}) V_{S,\Delta,\ell} \begin{pmatrix} \lambda_{tt\mathcal{O}} \\ \lambda_{ss\mathcal{O}} \end{pmatrix} + \sum_{\mathcal{O}_E} \lambda_{tt\mathcal{O}_E}^2 V_{T^2,E,\Delta,\ell} + \sum_{\mathcal{O}_O} \lambda_{ts\mathcal{O}_O}^2 V_{T^2,O,\Delta,\ell} + \sum_{\mathcal{O}} \lambda_{\mathcal{O}}^2 V_{T^4,\Delta,\ell} + \sum_{\mathcal{O}} \lambda_{tt\mathcal{O}}^2 V_{B,\Delta,\ell} + \sum_{\mathcal{O}} \lambda_{tt\mathcal{O}}^2 V_{A,\Delta,\ell} + \sum_{\mathcal{O}} \lambda_{tt\mathcal{O}}^2 V_{H,\Delta,\ell} + (\lambda_{tts} \ \lambda_{sss}) V_{\text{ext.}} \begin{pmatrix} \lambda_{tts} \\ \lambda_{sss} \end{pmatrix} = 0_{1 \times 10},$$

Here we have chosen to separate out the contributions proportional to the OPE coefficients of the external vector into a separate vector $V_{\text{ext.}}$. Since the A , T^4 , H and B representations cannot be exchanged in the new correlators the vectors V_A, V_{T^4}, V_H, V_B remain unaffected (apart from padding them with an appropriate number of zeros at the end). The entries of V_S become matrices since there are now contributions proportional to λ_{ttS}^2 , $\lambda_{tts}\lambda_{ssS}$ and λ_{sss}^2 . Furthermore, we split the traceless symmetric contribution into a \mathbb{Z}_2 even part coming from the $t \times t$ OPE and a \mathbb{Z}_2 odd part coming from $t \times s$ OPE. The \mathbb{Z}_2 even part remains identical to the vector V_{T^2} in equation 15. The $t \times s$ OPE exchanges traceless symmetric operators of both odd and even spin. The new vectors $V_S, V_{T^2,O}$ and $V_{\text{ext.}}$ are given by

$$V_S = \begin{pmatrix} \frac{1}{2}((N+N^2)-2)\mathcal{F}_{11}^{\Delta_{tt}\Delta_{tt}} \\ \mathbf{0} \\ \mathbf{0} \\ \mathbf{0} \\ \frac{1}{2}((N+N^2)-2)\mathcal{H}_{11}^{\Delta_{tt}\Delta_{tt}} \\ \mathbf{0} \\ \mathbf{0} \\ -\frac{1}{2}\mathcal{H}_{12}^{\Delta_{ss}\Delta_{ss}} \\ \frac{1}{2}\mathcal{F}_{12}^{\Delta_{ss}\Delta_{ss}} \\ \mathcal{F}_{22}^{\Delta_{ss}\Delta_{ss}} \end{pmatrix}, V_{T^2,O} = \begin{pmatrix} 0 \\ 0 \\ 0 \\ 0 \\ 0 \\ \mathcal{F}^{\Delta_{ts}\Delta_{ts}} \\ (-1)^L \mathcal{H}^{\Delta_{ts}\Delta_{ts}} \\ (-1)^L \mathcal{F}^{\Delta_{ts}\Delta_{ts}} \\ 0 \end{pmatrix}, V_{\text{ext.}} = \begin{pmatrix} \frac{1}{2}((n+n^2)-2)\mathcal{F}_{11}^{\Delta_{tt}\Delta_{tt}} \\ \mathbf{0} \\ \mathbf{0} \\ \mathbf{0} \\ \frac{1}{2}((n+n^2)-2)\mathcal{H}_{11}^{\Delta_{tt}\Delta_{tt}} \\ \mathbf{0} \\ \mathcal{F}_{11}^{\Delta_{ts}\Delta_{ts}} \\ \mathcal{H}_{11}^{\Delta_{ts}\Delta_{ts}} - \frac{1}{2}\mathcal{H}_{12}^{\Delta_{ss}\Delta_{ss}} \\ \mathcal{F}_{11}^{\Delta_{ts}\Delta_{ts}} + \frac{1}{2}\mathcal{F}_{12}^{\Delta_{ss}\Delta_{ss}} \\ \mathcal{F}_{22}^{\Delta_{ss}\Delta_{ss}} \end{pmatrix} \quad (17)$$

where we defined the matrices

$$(\mathcal{F}_{ij}^{\Delta_1,\Delta_2})_{mn} = \begin{cases} F^{\Delta_1,\Delta_2} & (i = n \wedge j = m) \vee (i = m \wedge j = n) \\ 0 & \text{else} \end{cases} \quad (18)$$

$$(\mathcal{H}_{ij}^{\Delta_1,\Delta_2})_{mn} = \begin{cases} H^{\Delta_1,\Delta_2} & (i = n \wedge j = m) \vee (i = m \wedge j = n) \\ 0 & \text{else.} \end{cases}$$

Finally, let us comment that the mixed $t-s$ setup does not break the map between

⁸The inclusion of $\langle tsts \rangle$ would add a new crossing symmetric $O(N)$ tensor structure where only the product of OPE coefficients $\lambda_{ttO}\lambda_{tsO}$ enter.

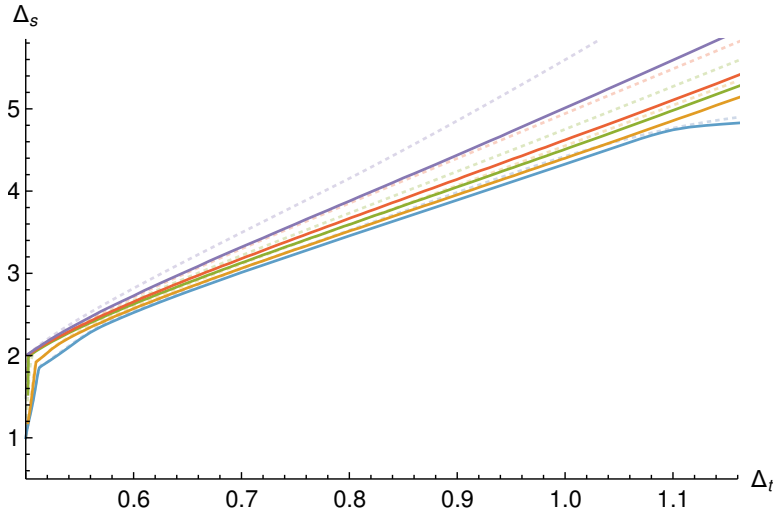


Figure 1: Bound on the dimension of the first singlet scalar. The blue, orange, green, red and purple lines correspond respectively to $N = 4, 5, 10, 20, 100$. These bounds have been obtained at $\Lambda = 27$. The dotted lines indicate the same bound at $\Lambda = 19$ and are included to illustrate the convergence. All bounds show a clear kink corresponding to the $O(N')$ model. An additional more dull kink is visible in the region $0.52 < \Delta_t < 0.58$. This kink gets less sharp and less precisely localized at larger N . For $N = 4$ an additional kink is visible around $\Delta_t = 1.1$. The bounds get strictly weaker for larger N .

the $O(N')$ vector bootstrap and the $O(N)$ traceless symmetric bootstrap and the same relations between positive functionals described in appendix C still hold.

3 A systematic study of general N

Here we present a systematic study of bounds on the dimension of the first operator in all representations for general N . Specifically we examine $N = 4, 5, 10, 20, 100$ and occasionally $N = 1000$ to study the asymptotic of certain kinks at large N . The bounds on the leading operators in the singlet representation are identical to the corresponding bounds found in the $O(N')$ -vector bootstrap⁹, where $N' = N(N + 1)/2 - 1$. For other representations there is not such relation.

3.1 Bounds on operator dimensions

Singlets

The bound on the dimension of the first singlet scalar Δ_S shows a clear kink corresponding to the $O(N')$ model under the identification $\phi^a \rightarrow t_{ij}$. In addition there is a second set of (dull) kinks in the region $0.52 < \Delta_t < 0.58$ whose exact location becomes less and less clear as N increase. An additional kink is visible around $\Delta_t \approx 1.1$

⁹This is proven in appendix C.

for $N = 4$. These bounds are shown in figure 1. In the scalar singlet sector we do not find any new interesting feature.

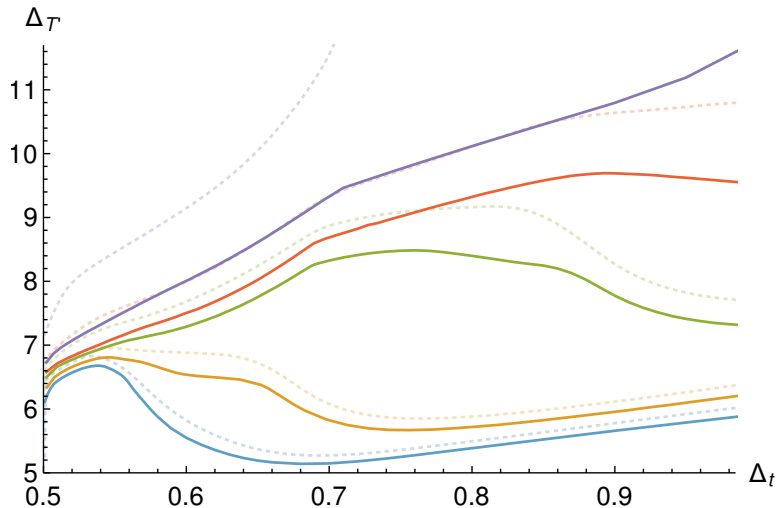


Figure 2: Bound on the dimension of the first spin-2 singlet after the stress tensor. The blue, orange, green, red and purple lines correspond respectively to $N = 4, 5, 10, 20, 100$. These bounds have been obtained at $\Lambda = 27$. The dotted lines indicate the same bound at $\Lambda = 19$ and are included to illustrate the convergence. For small N a peak is visible. For larger N the peak fades and the most discernible feature becomes a kink around $\Delta_t \approx 0.7$. The bounds get strictly weaker for larger N .

Next, we explored bounds on $\Delta_{T'}$, the dimension of the first spin-2 singlet after the stress tensor. For small N this bound shows a clear peak in the region $0.52 < \Delta_t < 0.58$. For larger N the peak fades and the most discernible feature becomes a kink around $\Delta_t \approx 0.7$. However it seems that especially for larger N the bounds are far from converged even at $\Lambda = 27$. These bounds are shown in figure 2.

It is a bit surprising that the bounds on the second spin-2 singlet are not very constraining. In fact, in most of CFTs based on a LGW description the next operator after the stress tensor has dimension $4 \lesssim \Delta_{T'} \lesssim 5$ [53, 54]. Similarly, in a gauge theory one expects to find an almost conserved spin-2 operator, coming from a combination the two stress tensors of the UV theory.¹⁰ We believe these bounds are far from optimal: we will see an explicit example for the case $N = 4$ in the next section.

Antisymmetric representation

More interesting features are visible in the bound on the first spin-1 antisymmetric vector after the conserved current, shown in figure 3. This is the first instance where the bounds are neither strictly weaker nor stronger when increasing N . At large Δ_t we see the usual behavior found for singlet operators, i.e. the bounds get weaker for

¹⁰In the limit of vanishing gauge coupling the theory contains two stress tensors, schematically $T_1^{\mu\nu} \sim \phi_i^\alpha \partial^\mu \partial^\nu \phi_i^\alpha$ and $T_2^{\mu\nu} \sim F^{\mu\rho} F_\rho^\nu$: in the IR one combination remains conserved while the orthogonal combination acquires an anomalous dimension.

larger N . Near the unitarity bound the trend is instead reversed. The bounds start quite above the value expected in a GFT, which however doesn't contain a conserved current. For $N = 4, 5$ we observe a sudden drop of the bound (a reversed kink) followed by a smooth bound. For larger values the kink fades away, and a second bump appears for $N \sim 10$ close to the unitarity bound.

All the bounds diverge as $\Delta_t \rightarrow 1$ and for large values of N an additional kink emerges.

The comparison of the bounds at $\Lambda = 19$ and $\Lambda = 27$ indicates a slow numerical convergence of the bounds for $\Delta_t \sim 1$, which get worse as N increases.

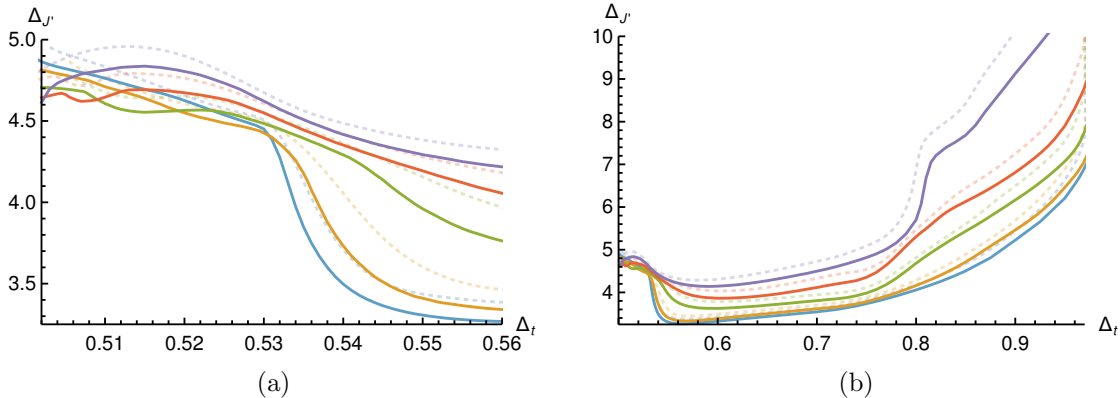


Figure 3: Both figures: Bound on the dimension of the first spin-1 antisymmetric vector after the conserved current. The blue, orange, green, red and purple lines correspond respectively to $N = 4, 5, 10, 20, 100$. The bounds have been obtained at $\Lambda = 27$. On the left: A zoom of the region $0.5 < \Delta_t < 0.58$. On the right: Overview of the same bound on $0.5 < \Delta_t < 1$. A second kink appears for $N = 10, 20, 100$ around $\Delta_t = 0.8$. The bounds diverge near $\Delta_t = 1$.

Box representation

Next we examine the bound on the dimension of the first scalar Box operator, see figure 4. For small N there are clear kinks in the region $0.54 \lesssim \Delta_t \lesssim 0.6$. Additionally there is a family of very sharp kinks for all N moving to the right towards $\Delta_t = 1$ as N increases. In this case the location of the kinks is quite stable when passing from $\Lambda = 19$ to $\Lambda = 27$ and the bounds seem to be converged.

It would be tempting to identify the family of kinks at large N with fixed points of gauge theories or $(A)RP^n$ models. Gauge theories discussed in section 1.3, however, are expected to contain operators with smaller dimension. On the other hand, $(A)RP^n$ are expected to have a large gap in this sector. In this case, one would expect $\Delta_t \sim 1 + O(1/N)$, while $\Delta_b \sim 4 + O(1/N)$. Unfortunately, the location of the kinks doesn't scale linearly with $1/N$, and it is unclear if they converge at all to $(\Delta_t, \Delta_b) = (1, 4)$ in the $\Lambda \rightarrow \infty, N \rightarrow \infty$ limit (see figure 18a in the appendix).

One possibility proposed in [55] is that bootstrap bounds for crossing equations based on a symmetry \mathcal{G}_N are in fact shaped by solutions with smaller symmetry $\mathcal{H}_M \subset \mathcal{G}_N$. This mechanism could explain the milder dependence on N : if for instance

the expansion parameter of \mathcal{H}_M is $1/M \sim 1/N^s$, with $s < 1$, then one would have a different scaling.

A different mechanism to produce kinks was proposed in [56]. In this case one could consider the difference between the 4pt function of a field $t_{ij} \sim \phi_i \phi_j + \dots$ made from two generalized free fields ϕ_i and the 4pt function of a generalized free field \mathcal{T}_{ij} . Since the former contains all the operators of the latter, it's possible to subtract the two 4pt functions and still have a decomposition in conformal blocks with positive coefficients. By subtracting the two, one can create large gaps and jumps in the bounds. This mechanism however would only explain kinks at $\Delta_t \geq 1$, as unitarity requires $\Delta_\phi \geq 1/2$.

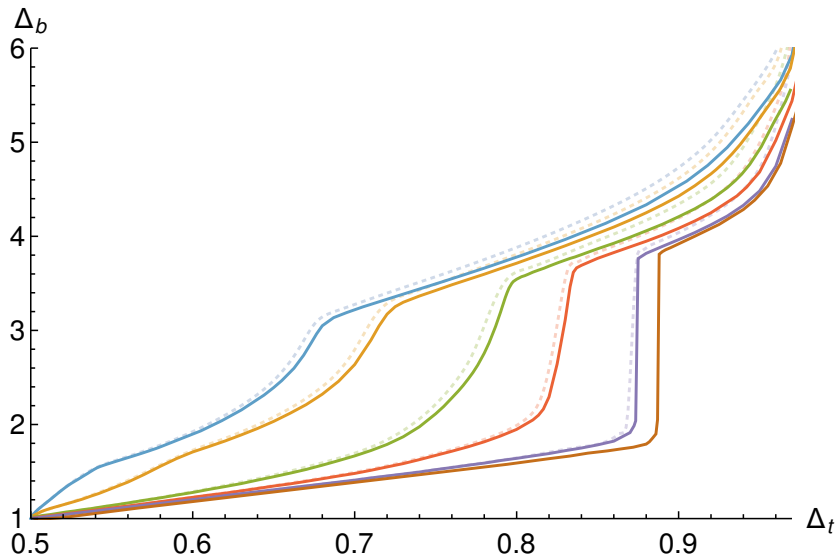


Figure 4: Bounds on the dimension of the first Box scalar. The blue, orange, green, red, purple and brown lines correspond respectively to $N = 4, 5, 10, 20, 100, 1000$. For $N = 4, 5$ there are kinks at $\Delta_t = 0.54$ and $\Delta_t = 0.60$ respectively. For larger N this kink disappears. A family of sharp kinks is visible for all N .

Hook representation

A similar family of kinks can be seen in the bound on the dimension of the first spin-1 Hook vector as is shown in figure 5. However, the location of the kink in Δ_t does not precisely match the location of the kinks in the bound on the first scalar Box operator.

Again it would be tempting to identify these kinks with CFTs admitting a large- N expansion but, as in the previous subsection, the dependence of the kink on $1/N$ doesn't seem to be linear or to converge to $(1, 4)$, at least at this value of Λ . In this case the situation is less clear, since the bounds seem farther from convergence in Λ , the features are less sharp, and they don't seem to strongly depend on N for $N \geq 1000$.¹¹

¹¹Neither the Hook nor the Box bound moves substantially when changing $N = 1000$ to $N = 10^{16}$ (this bound is not included in the figures).